Biosurface and Biotribology

WILEY

The Institution of Engineering and Technology

ORIGINAL RESEARCH OPEN ACCESS

Biomimetic Collagen Matrix With Aligned Architecture and Featured Stiffness Relative to Breast Cancer Cell Behaviour

Weilong Lin[1] | Manman Sun[1] | Ke Huang[1] | Hong Li[1,2]

[1]Department of Materials Science and Engineering, College of Chemistry and Materials Science, Jinan University, Guangzhou, China | [2]Engineering Research Center of Artificial Organs and Materials, Ministry of Education, Guangzhou, China

Correspondence: Hong Li (tlihong@jnu.edu.cn)

Received: 31 October 2025 | **Revised:** 22 April 2026 | **Accepted:** 23 April 2026

Keywords: architecture | collagen | invasion | MDA-MB-231 | stiffness

ABSTRACT

Cancer progression has been shown to be accompanied by alterations in physical features of its microenvironment. In the study, we fabricated an aligned collagen fibre matrix, whose architecture in both micro-level and nano-level was similar to that of the matrix found around the breast tumour tissue. The modulus of matrix exhibited a stiffness similarly to that found in metastatic breast tumour tissue. On the tough substrate, MDA-MB-231 cells presented an increased migration rate along the alignment of fibre. The biomechanical properties of tumour cells were explored in situ by AFM. The stiffness of a single MDA-MB-231 cell on the aligned matrix was reduced when compared with that on the nonaligned one. Wound healing assay showed that tumour cells with compliant modulus moved fast along the alignment of collagen fibre matrix. The in vitro model effectively mimicked the tumour cell behaviour, which would be helpful for new therapeutic strategies to detect cancer progress.

1 | Introduction

Breast cancer (BC) is the most common cancer in women [1]. Approximately 90% of BC cancer–induced deaths are a result of metastases [2]. To treat and predict BC progression, it is necessary to detect BC cell metastases as early as possible [3]. Recently, it was reported that the biophysical properties of breast cancer's microenvironments—including its biomechanical properties (stiffness, viscoelasticity and plasticity) [4] and extracellular matrix (ECM) structure (collagen architecture) [5]—play a critical role in mediating the behaviour of cancer cells. Notably, the physical properties of BC offer novel opportunities for achieving accurate and targeted therapeutic interventions.

Various physical cues, including biomechanical properties, architecture and anisotropy, act at the cell–ECM interface [6]. Collagen is the most popular ECM protein in and around the tumoral site. The tumour microenvironment often differs from the normal tissue due to elevated production and deposition of collagen [7–9]. In the context of BC, a heterogeneous ECM with a varying degree of local fibre alignment surrounds the breast tumour, which is typically from the normal breast tissue. The collagen fibres exhibit a highly straight, aligned morphology within the intra-tumoral region, while they adopt a wavy, corrugated architecture in the extra-tumoral region [5, 10]. Besides the ECM network, as a vital constituent of the local microenvironment, matrix stiffness is closely associated with the initiation and development of tumour. The matrix stiffness of the

The authors Weilong Lin and Manman Sun have equally contributed to the work.

tumour microenvironment had also been implicated in tumourigenesis [11]. Generally, the increase in the matrix elastic modulus is clinically proved to contribute to malignant transformation and poor survival of breast tumour [12]. The adjacent stroma displayed increased stiffness compared with normal tissues as a result of an increase in collagen density [13, 14]. An in vitro study also suggested that increased collagen density or concentration increased matrix stiffness and disrupted mammary morphogenesis [15]. Both matrix stiffness and featured texture of the BC microenvironment mediate cell–matrix interactions, resulting in cell adhesion and migration, therefore resulting in different prognostic outcomes. Therefore, an in vitro model–integrated architecture with biomechanical cue would provide hope for accurately predicting responses in BC metastases.

Most studies investigating the role of matrix stiffness on cell behaviour have primarily used polymer hydrogels, which are hydrated, mechanically tunable matrices usually based on crosslinked polymer strands of different molecular weights and crosslinking densities [16–18]. However, synthetic materials usually lack moieties for cellular adhesion to mimicking in vivo environment. What is more, the matrices still lack tunable architecture. Consequently, less is known about the effects of matrix stiffness on cellular behaviour in a physiologically relevant matrix where a heterogeneous ECM with varying local fibre alignment influences cell migration. The alignment architecture, which is a typical feature of the BC microenvironment, has been established by means of electrostatic spinning, microcontact printing, rotational alignment and so on [19–24]. With regard to the collagen self-assembled hierarchical structure, these collagen models are still far away from the natural ECM, from a nano-scale fibril to a geometrical tissue. The disadvantage would lead to the deviation and limitation of the examined results.

Herein, a collagen matrix with aligned fibrous nanostructure and featured stiffness was constructed via self-assembled way while we evaluated its affecting cell behaviours. The stiffness tomography and morphology of a single MDA-MB-231 cell on the collagen matrix were characterised in situ by AFM, which is less reported according to our knowledge. The trends of cell migration and behaviour guided by matrix architecture and biomechanical properties were explored. Validating the prediction of the aligned collagen model, this new approach to in vitro model of cancer cells will be beneficial to explore new therapeutic strategies.

2 | Materials and Methods

2.1 | Matrices' Preparation

100 × 100 mm glass slides were used as a substrate supporter in the experiments. Collagen I was extracted from rat tails via acid hydrolysis [25]. It was then dissolved in 0.5 mol/L acetic acid to prepare swelling solutions at concentrations of 20 mg/mL and 120 mg/mL. Bubbles in all solutions were removed by ultrasonic vibration for 30 min prior to use. For the aligned collagen matrix, 120 mg/mL collagen solution was dropped on clean glass slides, and the other cover glass was pressed and moved along the same direction for 15 times. As the 20 mg/mL collagen solution has low viscosity, the nonaligned collagen matrix was prepared by casting it directly into a petri dish. Then, all samples were put into the chemical hood at room temperature (RT) for 36 h to remove acidic residue. After the collagen was dried thoroughly, the collagen matrix was cut into similar sizes as the well of 24-well plates and 6-well plates for the subsequent experiments.

2.2 | Characterisation

The morphologies of collagen matrices were evaluated using a scanning electron microscope (SEM, TM3030, Japan). The alignment of collagen was measured by using CurveAlign-4.0. Contact angles of the collagen matrix surface were determined using a contact angle analyser (KRUSSDSA100, Germany). AFM analyses of the nonaligned and aligned collagen matrices were conducted in the ScanAsyst mode (BioScope Catalyst Bruker Instruments, Germany). After the samples were immersed in phosphate buffered saline (PBS, BI, pH = 7.4, [-] calcium, [-] magnesium) for 24 h, the images and Young's modulus of the collagen matrix were obtained under the following conditions: tap 150-Al-G silicon AFM probes at 16 × 16 pixels, scan area of 100 × 100 μm^2 and the scan rate of 0.3 Hz.

2.3 | In vitro Cell Assay

2.3.1 | Cell Culture and Seeding

MDA-MB-231 cells were purchased from Aili Biotechnology Co., Ltd (Shanghai, China) and cultured in Dulbecco's modified Eagle's medium (DMEM, Gibco) supplemented with 10% foetal bovine serum (FBS, Gibco) and 1% penicillin/streptomycin (Biological Industries, Israel) at the 37°C and 5% CO_2 environment. The collagen matrices were sterilised under Co^{60} with 15 KGy radiation in advance and placed on the 24-well plate bottoms; then, it was washed with sterilised PBS three times. MDA-MB-231 cells were seeded onto the collagen matrices, cell slides at an appropriate density and the cells cultured on cell slides were used as the control group throughout.

2.3.2 | Cell Adhesion and Proliferation

Cell proliferation was assessed via an MTT assay. MDA-MB-231 cells were seeded on 24-well plates contained the nonaligned and aligned collagen matrix. After the specified culture time points of 1, 3, 5, 7, 14 and 21 days, the collagen films were transferred to a new 24-well plate carefully and washed with PBS 1–2 times. New media were mixed with a 1 mL fresh medium, and 100 μL MTT (Sigma, USA) weas added to each well and incubated for 4 h at 37°C. Subsequently, the upper solution was discarded and 750 μL dimethyl sulfoxide was added (DMSO, Sigma) to dissolve the formazan crystals. 200 μL dissolved formazan supernatants were transferred into 96-well plates for the absorbance (OD) measurements using a microplate reader (Multiskan MK3, Thermo, USA) at 490 nm.

The cell adhesion on the collagen matrix was assessed by the MTT assay as well. MDA-MB-231 cells were seeded on the 24-well plates with collagen matrix and cell slides. After incubating 4 h, the OD values were measured. The control group was used as the reference to calculate the cell adhesion rate on the collagen matrices.

2.3.3 | Cell Morphology and Vinculin Observation

After culturing for 1, 3 and 5 days, the morphologies of MDA-MB-231 cells that adhered to the control and collagen matrices were observed by using a Zeiss LSCM 880 confocal microscope (Carl Zeiss, Germany). The cells were fixed with 4% paraformaldehyde (Leagene, China) for 15 min, washed with PBS three times, permeabilized with 0.5% Triton X-100 (Sigma) for 5 min and washed again. The nonspecific antigen binding sites were blocked with 1% bovine serum albumin (BSA, Sigma) for 1 h. The anti-vinculin antibody (1:250 diluted, Abcam) was used to stain the focal adhesion protein over night at 4°C; then, the cells were incubated with goat anti-rabbit IgG H&L (Cy3) preadsorbed secondary antibody (1:500 diluted, Abcam) for 30 min after washing. Subsequently, the F-actin of cells was stained with phalloidin labeled by fluorescein isothiocyanate for 1 h (1:200 diluted, Sigma-Aldrich), washed three times again. Eventually, the samples were incubated with DAPI (Sigma) for 5 min and then washed three times. Notably, all dyeing operations were executed under the conditions of protection from light at RT.

MDA-MB-231 cells' attachment was investigated by SEM after culturing for 3 days. Samples were fixed with 2.5% glutaraldehyde for 1 h at 4°C. The samples were then washed 3 times in PBS and dehydrated with a series of ethanol solutions (50%, 60%, 70%, 80%, 90% and 100%). After drying at RT, the cell morphologies of the samples were observed by SEM.

2.3.4 | Morphology and Stiffness of a Single Cell

The biophysical parameters (such as morphology, roughness and elastic modulus) changes of MDA-MB-231 cells on collagen matrices were visualised and analysed also via AFM. After MDA-MB-231 cells were cultured with nonaligned and aligned collagen and cell slides for 3 days, the cells were fixed with 4% paraformaldehyde for 15 min and then preserved in PBS to conduct AFM detection. Deflection Error and Force volume (FV) images of cells were acquired using arrays of 16 × 16 pixels under the following conditions: spring constant of 0.01 N/m, forward and reverse velocity of 2 μm/s and scan rate of 0.3 Hz. The morphologies of 20 cells selected randomly was scanned in the PBS of scan size of 70 × 70 μm^2. The arithmetic average roughness (Ra) and Young's modulus changes of MDA-MB-231 cells were calculated through scanning 20 areas of 5 × 5 μm^2 randomly. All plotted data were shown as the mean ± standard deviation (SD) of the histograms of the modulus extracted from all pixels in the FV images.

2.3.5 | Wound Healing Assay

The collagen matrices were cut into the similar sizes as the well of 24-well plates. After sterilising under Co60 radiation, the samples were placed in 24-well plates. Then, a specific ring chamber insert was placed on the collagen matrix, which was separated by a rectangular bar with a breadth of 2 mm. The direction of the rectangular bar was perpendicular to the collagen alignment. 2 mL cell suspensions were added into the insert at an appropriate density and incubated for 24 h. After cells spread completely, a "wound" line was formed in the middle of collagen matrix. Subsequently, chamber insert and medium were carefully removed and washed three times with PBS. Then, fresh media with 2% FBS were added to sustain cell migration while reducing the contribution of cell proliferation during the assay. The cells were incubated at 37°C and observed using CYTATION.3 imaging reader (BioTek, UK) every 2 h until the "wound" healed. Under the microscope, the cells that migrated into the cell-free zone formed by the 2-mm "wound" line were clearly evaluated.

2.4 | Statistical Analysis

All quantitative results were obtained from more than three samples. The data were expressed as the mean ± SD. Statistical analyses were calculated using SPSS18.0. $p < 0.05$ was considered statistically significant (*: $p < 0.05$ and **: $p < 0.001$).

3 | Results

3.1 | Architecture and Stiffness of Collagen Matrices

3.1.1 | Architecture

SEM images of collagen matrices were visualised in Figure 1. The nonaligned collagen matrix showed a random fibre structure under different magnifications in Figure 1a,b. The degree of collagen fibres alignment was shown in Figure 1c, and there was no preferential direction of collagen fibre spread for the nonaligned matrix. As shown in Figure 1d, the aligned collagen matrix exhibits a regular striated morphology characterised by parallel strips separated by gaps ranging from 60 to 100 μm. Further, the zoomed in view in Figure 1e shows that collagen fibre in a diameter of a nano-scale parallelled closely and aligned in a specific direction, which is remarkably similar to the tumoral microenvironment [26]. The aligned fibres corrugated along the directions of 45° (in red arrow) and 105° (in yellow arrow), which formed the defined strips as shown in Figure 1d,e (yellow dotted line). The orientation distribution calculated in Figure 1f confirms this pattern, with fibres concentrating in two angular ranges of 30°~60° and 105°, aligning perfectly with the visual data in Figure 1e.

3.1.2 | Stiffness Tomography of Collagen Matrices

The collagen matrices were immersed in PBS, and their microtopography and Young's modulus were measured by AFM. Figure 2a–d showed 2D and 3D morphologies of the collagen matrices. As shown in Figure 2c–d, the aligned matrix retained its aligned structure in PBS, whereas the nonaligned matrix displayed a random fibre arrangement. The average surface roughnesses (Ra) of the nonaligned and aligned collagen matrices were 2.13 ± 0.32 nm and 0.46 ± 0.11 nm, respectively, indicating a statistically significant difference and a smoother surface for the aligned matrix. This result is corroborated by the 3D topographies presented in Figure 2b,d. The histograms of Young's modulus with Gaussian fitting curves for both matrices are shown in Figure 2g–h. The average stiffness of the nonaligned matrix and the aligned one were 2.74 ± 0.94 MPa and 3.03 ± 1.58 MPa, respectively, which kept the differences similar to that of benign and malignant lesions in vivo [27, 28]. Notably, the modulus of the aligned collagen matrix exhibited bimodal peaks as shown in Figure 2h, which may be attributed to the surface undulations corresponding to its corrugated structure. Although wavy collagen fibres have been observed in

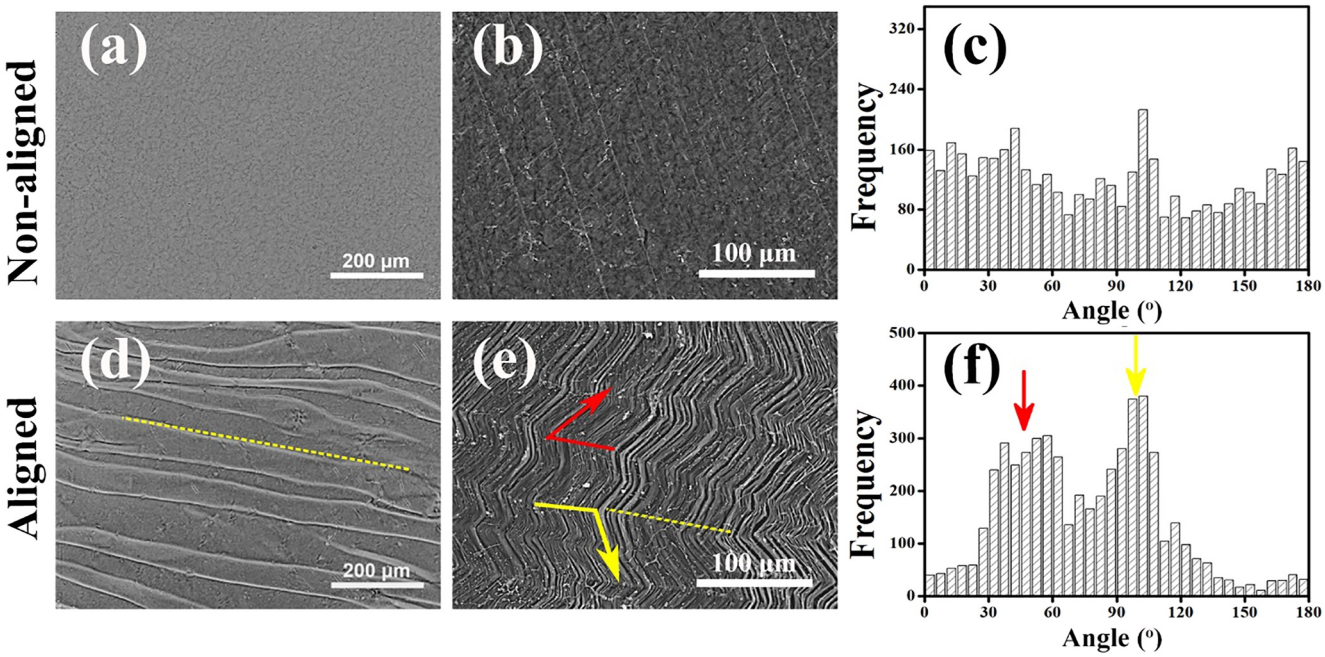

FIGURE 1 | SEM micrographs and alignment analyses of collagen matrices. (a, b, d and e) Morphologies of nonaligned and wavy aligned collagen matrices under × 200 and × 500. (c and f) The nonaligned and wavy aligned collagen fibres alignments corresponded with (b) and (e).

tumour sites, such a distinct bimodal mechanical property has, to our knowledge, not been previously reported [26, 29, 30]. Besides, as shown in Figure 2e, the contact angle value of the aligned matrix was only 81.5 ± 2.11° and was minimum among the samples under dry condition. The result indicated that the aligned collagen was more hydrophilic than others.

3.2 | Proliferation and Adhesion of MDA-MB-231 Cells

Cells' proliferation and adhesion were measured by MTT assay. After incubating MDA-MB-231 cells on the collagen matrix for 1, 3, 5, 7, 14 and 21 days, the number of cells kept an excellent increase as shown in Figure 3a. A higher proliferation on the collagen matrices was statistically different from the control group (TCP, tissue culture plate). Notably, no statistically significant difference was detected between the aligned and nonaligned collagen groups at the examined time points. It means that cell proliferation showed no significant dependence on fibre alignment according to our study.

Regarding cell adhesion on the matrices, it could be seen that the attached cell numbers on the collagen matrices were lower than that on the control one from Figure 3b, but the cell number on the aligned matrix was still higher than that on the nonaligned one.

3.3 | Morphology and Vinculin of MDA-MB-231 Cells

It can be seen from the images Figures 4 and 5a that both F-actin (green panel) and vinculin (red panel) of the cells exhibited different structures and distributions on various substrates. Especially in Figure 4a,d,g,j, the F-actin structure was irregular when cells were cultured on the control group, whereas the cells on the collagen matrices present in fewer pseudopods and nattier cytoskeleton contours with stretched morphology as shown in Figure 4. Combined with the SEM images of Figure 4j–l, we could also clearly observe that the cells stretched no specific orientation on the nonaligned collagen matrix, but the cells on the aligned matrix stretched along the alignment of collagen fibre (red arrow). Although obvious micro-strips existed in the aligned matrix (Figure 1d), the cells still grew along the elongation of collagen fibre. The result means that the cells would be guided by the nano-architecture of its supporting substrate and further migrate along the alignment of nanofiber. Based on the quantitative analyses of the average projected area and aspect ratio of MDA-MB-231 cells (Figure 5b,c), the lowest spread area and the largest aspect ratio were contributed to the cells on the aligned collagen matrix, which further confirmed that the cells stretched in an elongated way on the matrix.

As shown in the images of Figure 5a, the vinculins of MDA-MB-231 cells were mostly distributed at the perinuclear areas where they were compactly connected with the substrate. Vinculin fluorescence intensities of the single cell that had been cultured on different matrices for 1, 3 and 5 days were similar (Figure 5d). When MDA-MB-231 cells cultured on the collagen matrices, the aligned collagen matrix was more positive in enhancing vinculin expression than the nonaligned one. Although more vinculin of MDA-MB-231 cells was secreted in the aligned collagen template, it was less distributed in the pseudopodia according to Figure 5a.

3.4 | Stiffness Tomography of a Single MDA-MB-231 Cell in situ

As shown in Figure 6a,e,i, the morphology of a single cell was scanned in situ via AFM. The cell with a polygon structure spread very well on the control group. However, the elongated

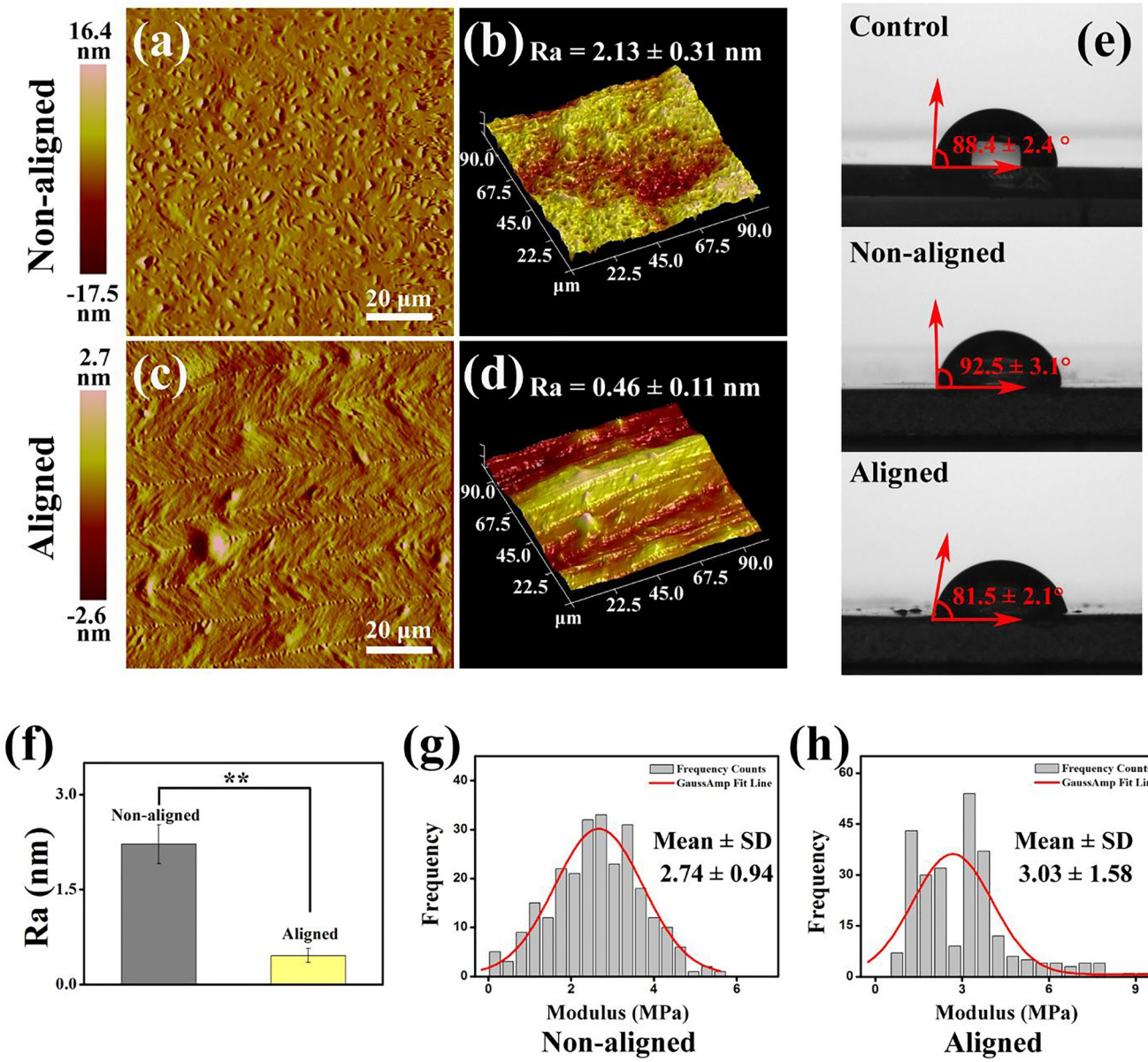

FIGURE 2 | Physicochemical properties of collagen matrices characterised by AFM and the contact angle analyser. (a–d) 2D and 3D topographies of nonaligned and wavy aligned collagen matrices. (e) The contact angles of different matrices. (f) Statistical analysis of Ra values of (b) and (d). (g and h) Young's modulus histograms and mean ± SD values of nonaligned and wavy aligned collagen matrices. (**$p < 0.001$).

cell still presented on the nonaligned collagen fibre. Meanwhile, it was observed that the single cell had fewer pseudopods and smaller spreading areas and tended to be in a more elongated morphology on the aligned matrix. Further, from the 3D topographies as shown in Figure 6b,f,j, it was noted that the single cell cultured on the aligned collagen had the smoothest surface appearance, whereas the cells cultured on the nonaligned collagen and control were especially rugged. Figure 6c,g,k were the hot maps of Young's modulus of the individual cells. Figure 6d,h,l statistically showed the stiffness of the single MDA-MB-231 cells in the same areas, respectively. The average modulus values of the single cells cultured on the control, nonaligned and aligned collagen matrices were 22.67 ± 6.51 kPa, 16.76 ± 5.95 kPa and 10.92 ± 3.80 kPa, respectively. As a result, the MDA-MB-231 cells on the aligned collagen matrix showed the lowest Young's modulus. That is to say, due to the alignment of collagen matrix, the MDA-MB-231 cells were more compliant although the modulus of the aligned matrix was tougher.

3.5 | Migration of MDA-MB-231 Cells

Figure 7a showed the comparison of cell migration in real time on the collagen matrices. Yellow straight lines in Figure 7a were used to delineate the cell migration distance. Firstly, the cell migration distances were significantly extensive on the collagen matrices than the control one. Secondly, the average migration rates (Figure 7c) of cells on the control, nonaligned and aligned collagen were 12.29 ± 1.19, 15.97 ± 0.93 and 19.52 ± 1.12 μm/h, respectively. MDA-MB-231 cells on the aligned collagen matrix migrated faster than the other two. Thirdly, cells migrated along the direction of collagen fibres as shown in Figure 7b basically

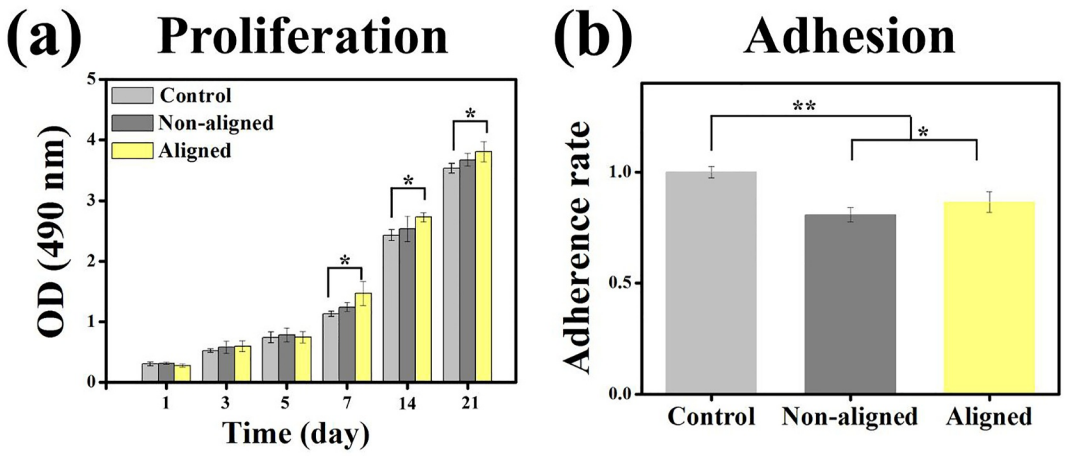

FIGURE 3 | The proliferation (a) and adhesion (b) of MDA-MB-231 cells cultured on different matrices. ($n > 10$, $^{*}p < 0.05$ and $^{**}p < 0.001$). (Control: TCP).

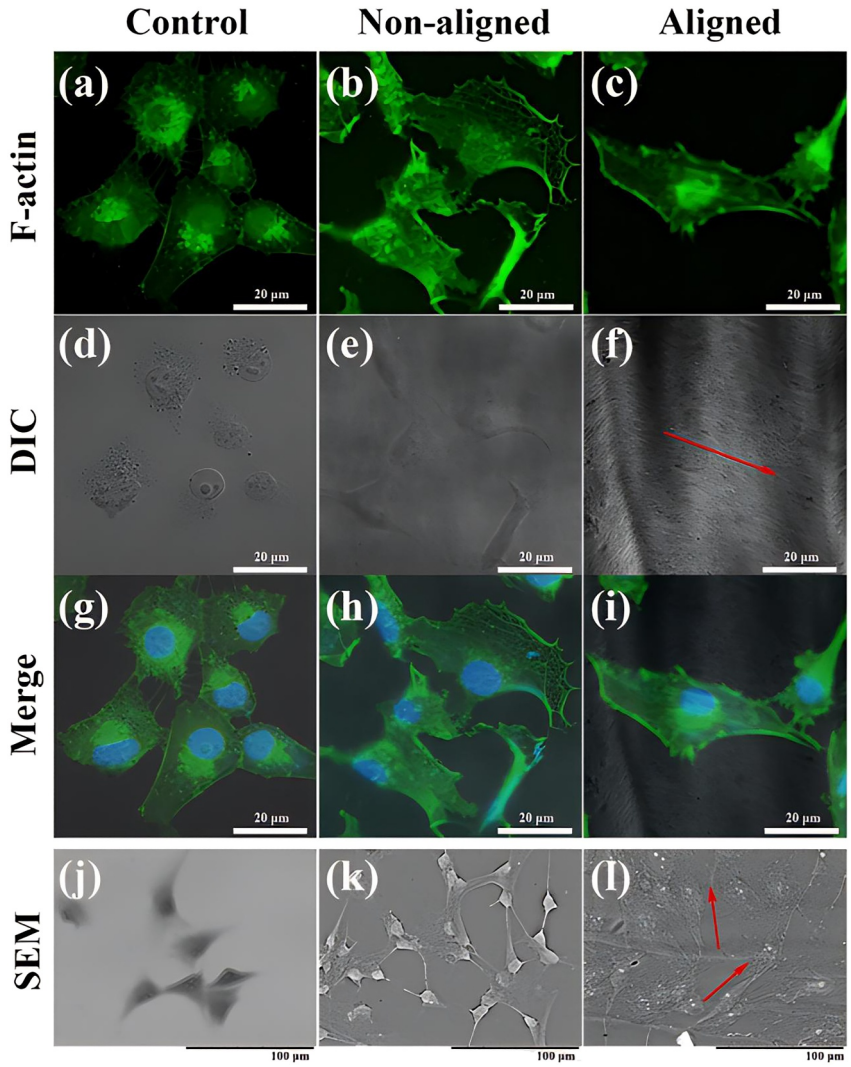

FIGURE 4 | Morphology and orientation of MDA-MB-231 cells cultured on different collagen matrices for 3 days. (a–i) LSCM images of the spread of a single cell (blue: nucleus and green: F-actin). (j–l) SEM images of the MDA-MB-231 cells.

covered the whole field of vision within 24 h. The results indicated that the alignment of collagen fibre had a pronounced effect on the directional migration of MDA-MB-231 cells, so had the rate of migration. It implies that the alignment of collagen fibre might be an important factor of breast cancer cell metastasis.

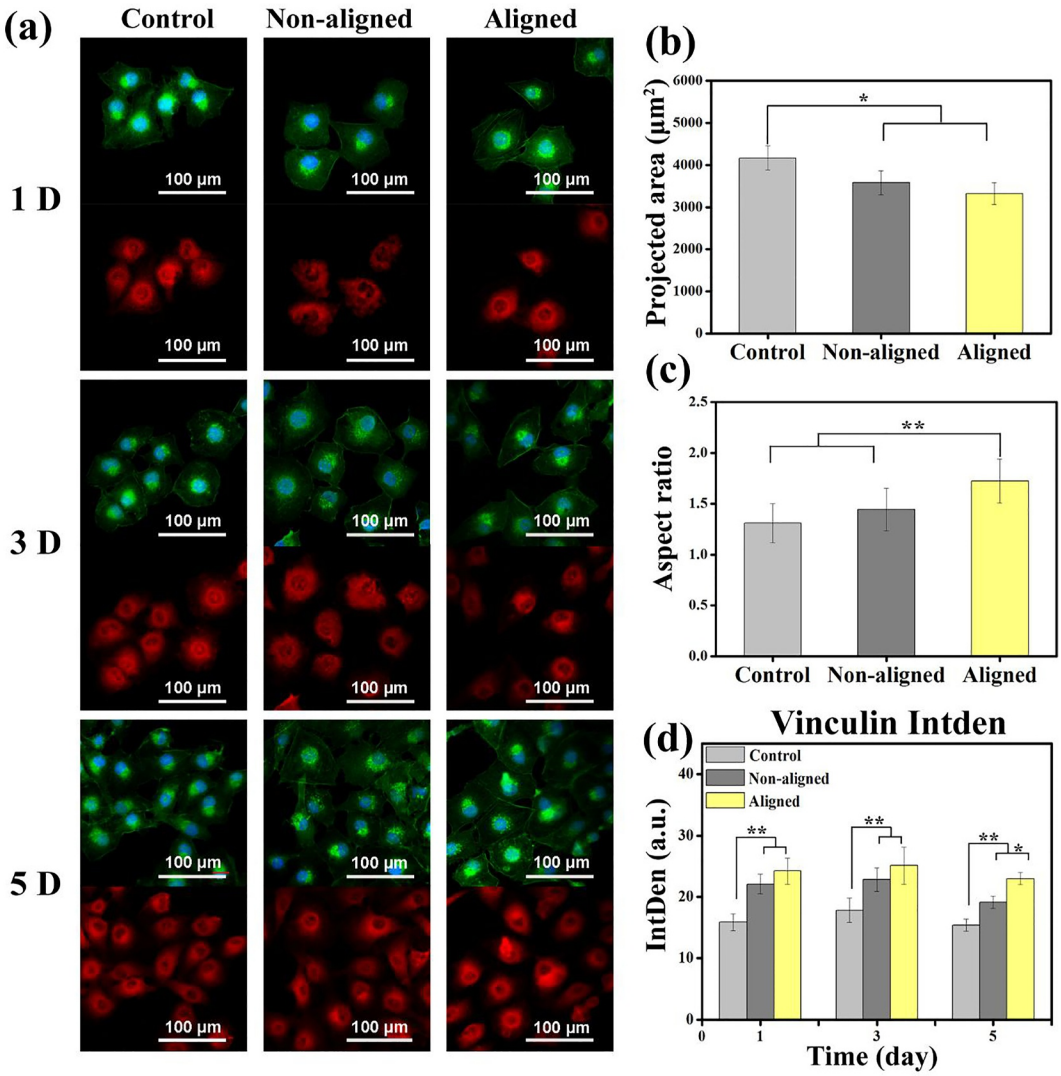

FIGURE 5 | Morphological observation and statistical analysis of MDA-MB-231 cells cultured on different matrices. (a) LSCM images of the spread and vinculin status of MDA-MB-231 cells for different days (blue: nucleus, green: F-actin and red: vinculin). (b and c) The projected areas and aspect ratios of MDA-MB-231 cells cultured on different matrices for 3 days. (d) The fluorescence intensities of vinculin at different days. ($n > 10$, $^{*}p < 0.05$ and $^{**}p < 0.001$).

4 | Discussion

Aligned collagen fibres with periodic corrugation structures contribute to maintaining the stiffness of cancer tissue [30, 31]. Substrates with high stiffness and aligned structures have been prepared by regulating the temperature of elastic substrates [32, 33]. However, there have been few studies [34, 35] to establish dense collagen architecture with periodic structure to mimic the natural ECM of breast cancer. In the study, after directional shearing of high concentration collagen gel, we successfully fabricated the collagen matrix with highly aligned periodic corrugation structure, while the nonaligned matrix was prepared using low concentration collagen gel. This difference in concentration was necessary to achieve distinct architectures: Only high-concentration collagen could form dense and aligned fibrous structures under shearing, whereas low-concentration collagen was too fluid to generate alignment. In particular, the aligned collagen matrix contained no other ingredients, such as glutaraldehyde and genipin crosslinker [36, 37]. Thus, the model was compositionally and structurally similar to the natural ECM of cancer tissue. Besides, according to the results of AFM, the modulus of the aligned collagen matrix was significantly higher than that of the nonaligned one (Figure 2), which kept accord with the result of breast tumour microenvironment [38]. In other words, the prepared aligned collagen matrix is not only consistent with the tumour ECM in terms of aligned structure and composition, but also possessed the similar biophysical property as the breast tumour microenvironment.

Fibre alignment have been shown to have a significant effect on cellular behaviour [39]. Studies of cells cultured in matrices with aligned fibres have revealed cells polarised and aligned with respect to the alignment [39, 40] and that alignment was associated with increased migration and directionality [15, 20, 22]. The direction of MDA-MB-231 cell migration corresponded to the orientation of the collagen fibres (Figure 7b), although the matrix with a wavy alignment is different from those with a straight parallelled alignment [26, 30]. It has been demonstrated that the aligned fibres may also afford cells less spatial

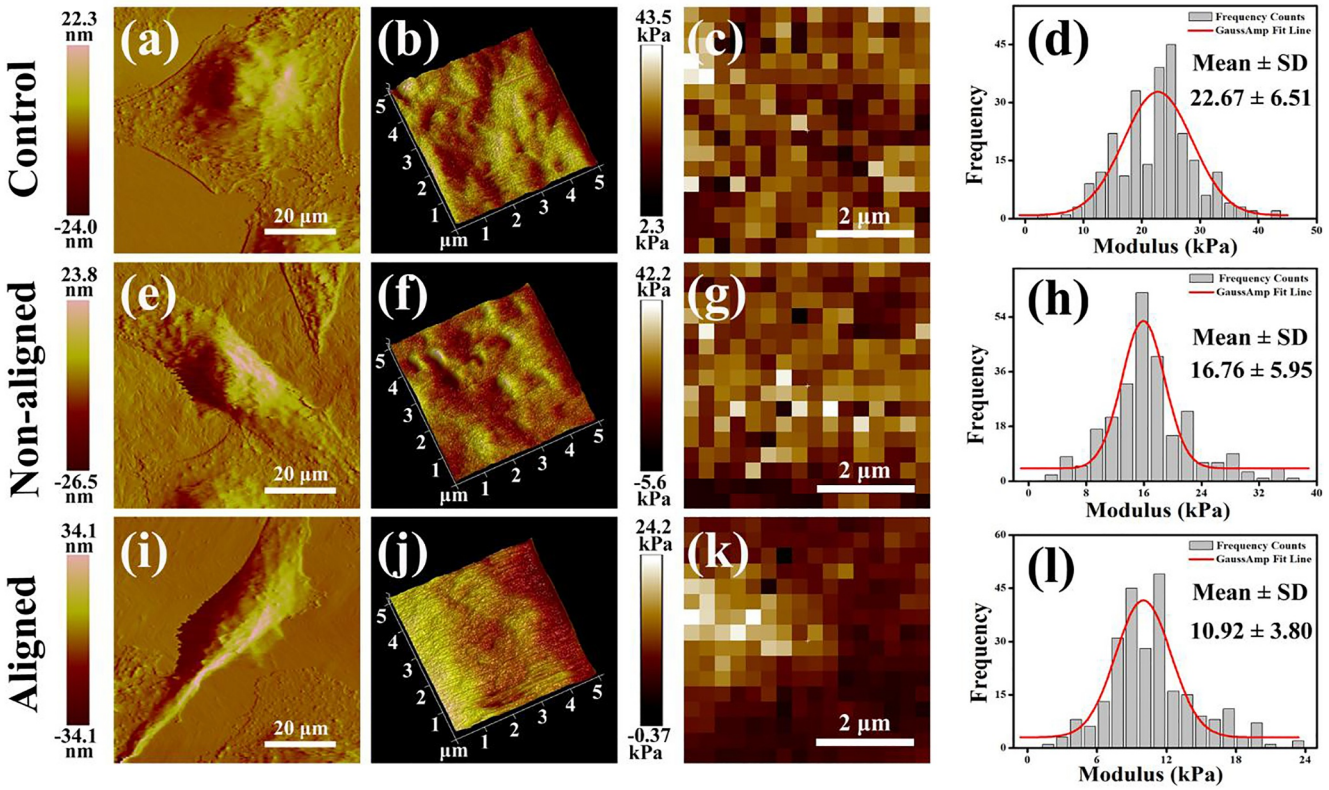

FIGURE 6 | Behaviours of MDA-MB-231 cells on different collagen matrices under the PBS. (a, e and f) Variations of single cellular morphology. (b, f and j) 3D topographies of cells for the partial regions. Hot maps (c, g and k) and histograms (d, h and l) of Young's modulus distribution for MDA-MB-231 cells.

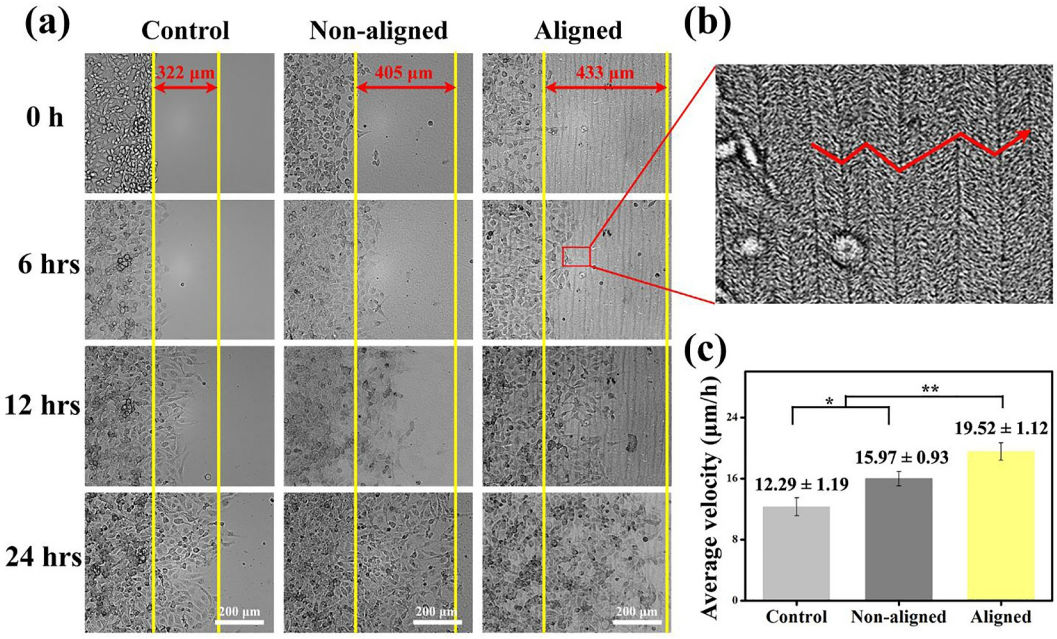

FIGURE 7 | Migration of MDA-MB-231 cells on different collagen matrices. (a) The migration distance of the cells at continuous time points. (b) Migration direction of the cells cultured on an aligned collagen matrix. (c) Average migration rates of the cells. ($n = 5$, $^{*}p < 0.01$ and $^{**}p < 0.001$).

impedance and thereby enhance migration [41], which is consistent with the results shown in Figure 7a,c. In other words, the tumour cells would move fast and directionally at the juxta-tumoral region. Generally, metastatic breast cancer cells mainly migrated along the orientation of the collagen fibre and achieved metastasis through vessel invasion. When tumour cells acquired the capacity to move around and invade other tissues, the aligned collagen fibre provided the orientation and accelerated cell migration [42, 43]; this phenomenon is called "contact guidance". The migration of cancer cells away from the

primary tumour and into healthy tissue is driven partly by contact guidance, or directed migration in response to the aligned extracellular matrix. It also implied that the migration rate of metastatic cells can be minimised through interfering with the tumour microenvironment.

The alignment of collagen fibres is contributed to the changes of matrix stiffness, and the biomechanical properties of substrate materials also plays a vital role in regulating the behaviours of cancer cells [15, 44]. As in the previous studies, the adhesion, spreading, proliferation and migration of tumour cancer cells significantly increased with the matrix stiffness in vitro [45–47]. Compared with the nonaligned one, the MDA-MB-231 cells aligned with collagen matrix with a higher modulus and had a superior adhesion (Figure 3b) and migration (Figure 7). Consistently, cells on the stiffer matrix accumulated more vinculin around the nucleus. This is known to elevate Rho-dependent cytoskeletal tension compared to cells on softer substrates [48], potentially facilitating stronger matrix attachment. Meanwhile, a stiffer matrix contributes to stronger contractility, so the contraction force on the surface of the matrix is transmitted to the nucleus through the stress fibres [49, 50]. The stronger the contraction force, the greater the cell movement, so a higher cell migration was observed on the aligned matrix.

However, the specific role of ECM stiffness in guiding cell migration remains incompletely understood. To further understand why the cell migration was accelerated along the alignment of collagen fibre, we analysed in detail a single MDA-MB-231 cell by AFM in situ. Comparatively, MDA-MB-231 cells on the aligned matrix had the minimum projected area (Figure 6i), the lowest roughness (Figure 6j) and the smallest Young's modulus (Figure 6l). Just as the previous analysing of one-fold cancer cell, cancer cells were more compliant [51]. Furthermore, the lower elastic modulus of the cells likely facilitates their deformation and migration [28, 38, 52], even though the aligned fibre substrate itself has a higher modulus.

As discussed previously [53], stiff substrates support adhesion-dependent rapid mesenchymal migration of tumour cells by enhancing cellular contractile tension and stabilising focal adhesions as we showed in Figures 5 and 7. Generally, the intrinsic mechanical property of cancer cells is dynamically modulated by extracellular matrix stiffness. Upon stiff substrates, elevated RhoA/ROCK-dependent actomyosin contractility facilitates F-actin polymerisation, accompanied by force-induced vinculin activation [54, 55]. The reinforced cytoskeletal network collectively increases cellular elastic modulus. However, our result indicated that MDA-MB-231 cells exhibit the lowest Young's modulus on the stiffer collagen matrix. Several studies reported that on extremely stiff substrates (50–100 kPa, pathological), excessive mechanical stress triggers F-actin disassembly, focal adhesion disruption and cytoskeletal fluidisation, leading to cell softening [56, 57]. It is supposed that the stiffer matrix may lead to either less polymerised or fragmental F-actin and then drive cell softening. Although the constructed model has a modulus of 3 MPa, far higher than extremely stiff substrates, the behaviour of cells are complex, which need to be explored deeply and systematically.

In summary, the prepared collagen matrix was compositionally, structurally and biomechanically consistent with the microenvironment of breast tumour and could simulate the behaviours of MDA-MB-231 cells in vitro. The study not only supports clinical biopsies of breast cancer metastatic cell invasion, but also reveals the process and mechanism of ECM-enhanced cell migration during intravasation in a biophysical way. It should be noted that this simplified 2D Type I collagen matrix has certain limitations, as it cannot fully replicate the complex 3D tumour microenvironment containing multiple ECM components and stromal cells. Nevertheless, it allows us to independently reveal the key role of collagen arrangement and matrix stiffness in regulating the behaviour of breast cancer cells. Future research can focus on constructing 3D biomimetic models by integrating multiple ECM proteins and stromal cells. It is strongly argued that a potential therapy tuning with a biophysical way could be considered, in which the alignment of ECM fibres in the tumour microenvironment might be altered to minimise the intravasation rate of metastatic cells.

5 | Conclusion

In the study, the aligned collagen fibrous matrix that was compositionally, structurally and biomechanically similar to the microenvironment metastatic breast tumour was prepared. MDA-MB-231 cells exhibited a high degree of directional response to the alignment of collagen fibre during the cell movement. By AFM nanoindentation, a significantly lower Young's modulus value for a single cell on the aligned matrix was detected, a finding that has been rarely reported. The lower stiffness of the cells made them easy to migrate and further affirmed the MDA-MB-231 cells' better migrations on the aligned collagen matrix. Our results provided biomechanical evidence to support the tumour microenvironment of local collagen fibre alignment in guiding cell intravasation. It indicates that the aligned collagen matrix is promising for studying the migration mechanism of breast cancer in vitro and exploring a new therapy to minimise breast tumour metastasis.

Acknowledgements

This work was supported by National Natural Science Foundation of China (Grant No. 31971284), Guangdong Basic and Applied Basic Research Foundation (Grant No. 2024A1515013268) and The Fundamental Research Funds for Central Universities, China (Grant No. 21624101).

Conflicts of Interest

The authors declare no conflicts of interest.

Data Availability Statement

Data are provided within the manuscript files.

References

1. E. Nolan, G. J. Lindeman, and J. E. Visvader, "Deciphering Breast Cancer: From Biology to the Clinic," *Cell* 186, no. 8 (2023): 1708–1728, https://doi.org/10.1016/j.cell.2023.01.040.

2. M. Botlagunta, M. D. Botlagunta, M. B. Myneni, et al., "Classification and Diagnostic Prediction of Breast Cancer Metastasis on Clinical Data Using Machine Learning Algorithms," *Scientific Reports* 13, no. 1 (2023): 485, https://doi.org/10.1038/s41598-023-27548-w.

3. M. Park, D. Kim, S. Ko, A. Kim, K. Mo, and H. Yoon, "Breast Cancer Metastasis: Mechanisms and Therapeutic Implications," *International Journal of Molecular Sciences* 23, no. 12 (2022): 6806, https://doi.org/10.3390/ijms23126806.

4. E. C. Filipe, S. Velayuthar, A. Philp, et al., "Tumor Biomechanics Alters Metastatic Dissemination of Triple Negative Breast Cancer via Rewiring Fatty Acid Metabolism," *Advanced Science* 11, no. 23 (2024): 2307963, https://doi.org/10.1002/advs.202307963.

5. M. Franchi, V. Masola, M. Onisto, et al., "Ultrastructural Changes of the Peri-Tumoral Collagen Fibers and Fibrils Array in Different Stages of Mammary Cancer Progression," *Cells* 14, no. 13 (2025): 1037, https://doi.org/10.3390/cells14131037.

6. S. C. Schüler, Y. G. Liu, S. Dumontier, et al., "Extracellular Matrix: Brick and Mortar in the Skeletal Muscle Stem Cell Niche," *Frontiers in Cell and Developmental Biology* 10 (2022): 1056523, https://doi.org/10.3389/fcell.2022.1056523.

7. C. E. Barcus, K. A. O'leary, J. L. Brockman, et al., "Elevated Collagen-I Augments Tumor Progressive Signals, Intravasation and Metastasis of Prolactin-Induced Estrogen Receptor Alpha Positive Mammary Tumor Cells," *Breast Cancer Research* 19, no. 1 (2017): 9, https://doi.org/10.1186/s13058-017-0801-1.

8. A. M. A. Romer, M. L. Thorseth, and D. H. Madsen, "Immune Modulatory Properties of Collagen in Cancer," *Frontiers in Immunology* 12 (2021): 791453, https://doi.org/10.3389/fimmu.2021.791453.

9. W. H. Huang, S. L. Ding, X. Y. Zhao, et al., "Collagen for Neural Tissue Engineering: Materials, Strategies, and Challenges," *Materials Today Bio* 20 (2023): 100639, https://doi.org/10.1016/j.mtbio.2023.100639.

10. P. Guimaraes, M. Morgado, and A. Batista, "On the Quantitative Analysis of Lamellar Collagen Arrangement With Second-Harmonic Generation," *Biomedical Optics Express* 15, no. 4 (2024): 2666–2680, https://doi.org/10.1364/boe.516817.

11. M. R. Ng and J. S. Brugge, "A Stiff Blow From the Stroma: Collagen Crosslinking Drives Tumor Progression," *Cancer Cell* 16, no. 6 (2009): 455–457, https://doi.org/10.1016/j.ccr.2009.11.013.

12. T. T. Wu, S. S. Xiong, M. M. Chen, et al., "Matrix Stiffening Facilitates the Collective Invasion of Breast Cancer Through the Periostin-Integrin Mechanotransduction Pathway," *Matrix Biology* 121 (2023): 22–40, https://doi.org/10.1016/j.matbio.2023.05.006.

13. T. Koorman, K. A. Jansen, A. Khalil, et al., "Spatial Collagen Stiffening Promotes Collective Breast Cancer Cell Invasion by Reinforcing Extracellular Matrix Alignment," *Oncogene* 41, no. 17 (2022): 2458–2469, https://doi.org/10.1038/s41388-022-02258-1.

14. Y. Q. Liu, X. M. Yao, Y. B. Zhao, et al., "Mechanotransduction in Response to ECM Stiffening Impairs cGAS Immune Signaling in Tumor Cells," *Cell Reports* (2023): 42.

15. B. Lanfer, U. Freudenberg, R. Zimmermann, D. Stamov, V. Körber, and C. Werner, "Aligned Fibrillar Collagen Matrices Obtained by Shear Flow Deposition," *Biomaterials* 29, no. 28 (2008): 3888–3895, https://doi.org/10.1016/j.biomaterials.2008.06.016.

16. J. N. Beck, A. Singh, A. R. Rothenberg, J. H. Elisseeff, and A. J. Ewald, "The Independent Roles of Mechanical, Structural and Adhesion Characteristics of 3D Hydrogels on the Regulation of Cancer Invasion and Dissemination," *Biomaterials* 34, no. 37 (2013): 9486–9495, https://doi.org/10.1016/j.biomaterials.2013.08.077.

17. H. L. Hiraki, D. L. Matera, W. Y. Wang, et al., "Fiber Density and Matrix Stiffness Modulate Distinct Cell Migration Modes in a 3D Stroma Mimetic Composite Hydrogel," *Acta Biomaterialia* 163 (2023): 378–391, https://doi.org/10.1016/j.actbio.2022.09.043.

18. I. Arciero, S. Buonvino, V. Palumbo, M. Scimeca, and S. Melino, "A 3D-Printable Cell Array for in Vitro Breast Cancer Modeling," *International Journal of Molecular Sciences* 25, no. 23 (2024): 13068, https://doi.org/10.3390/ijms252313068.

19. W. J. Han, S. H. Chen, W. Yuan, et al., "Oriented Collagen Fibers Direct Tumor Cell Intravasation," *Proceedings of the National Academy of Sciences of the United States of America* 113, no. 40 (2016): 11208–11213, https://doi.org/10.1073/pnas.1610347113.

20. J. J. Campbell, A. Husmann, R. D. Hume, C. J. Watson, and R. E. Cameron, "Development of Three-Dimensional Collagen Scaffolds With Controlled Architecture for Cell Migration Studies Using Breast Cancer Cell Lines," *Biomaterials* 114 (2017): 34–43, https://doi.org/10.1016/j.biomaterials.2016.10.048.

21. A. Ray, O. Lee, Z. Win, et al., "Anisotropic Forces From Spatially Constrained Focal Adhesions Mediate Contact Guidance Directed Cell Migration," *Nature Communications* 8, no. 1 (2017): 14923, https://doi.org/10.1038/ncomms14923.

22. G. R. Jin, R. Y. He, B. Y. Sha, et al., "Electrospun Three-Dimensional Aligned Nanofibrous Scaffolds for Tissue Engineering," *Materials Science & Engineering, C: Materials for Biological Applications* 92 (2018): 995–1005, https://doi.org/10.1016/j.msec.2018.06.065.

23. V. A. Zavareh, L. Rafiee, M. Sheikholeslam, et al., "Three-Dimensional Models: A Promising Tool to Scale-Up Breast Cancer Research," *ACS Biomaterials Science & Engineering* 8 (2022): 4648–4672, https://doi.org/10.1021/ACSBIOMATERIALS.2C00277.

24. P. Li, H. Y. Zhou, R. Yan, et al., "Aligned Fibrous Scaffolds Promote Directional Migration of Breast Cancer Cells Caveolin-1/YAP-Mediated Mechanosensing," *Materials Today Bio* 28 (2024): 101245, https://doi.org/10.1016/j.mtbio.2024.101245.

25. N. Rajan, J. Habermehl, M. F. Coté, C. J. Doillon, and D. Mantovani, "Preparation of Ready-To-Use, Storable and Reconstituted Type I Collagen From Rat Tail Tendon for Tissue Engineering Applications," *Nature Protocols* 1, no. 6 (2006): 2753–2758, https://doi.org/10.1038/nprot.2006.430.

26. A. Brabrand, I. I. Kariuki, M. J. Engstrom, et al., "Alterations in Collagen Fibre Patterns in Breast Cancer. A Premise for Tumour Invasiveness?," *Apmis* 123 (2015): 1–8, https://doi.org/10.1111/apm.12298.

27. A. Athanasiou, A. Tardivon, M. Tanter, et al., "Breast Lesions: Quantitative Elastography With Supersonic Shear Imaging-Preliminary Results," *Radiology* 256, no. 1 (2010): 297–303, https://doi.org/10.1148/radiol.10090385.

28. R. Rezk, R. Marín-García, and A. K. B. Gad, "The Fibrillar Matrix: Novel Avenues for Breast Cancer Detection and Treatment," *Engineering* 7, no. 10 (2021): 1375–1380, https://doi.org/10.1016/j.eng.2021.04.024.

29. G. Falzon, S. Pearson, and R. Murison, "Analysis of Collagen Fibre Shape Changes in Breast Cancer," *Physics in Medicine and Biology* 53, no. 23 (2008): 6641–6652, https://doi.org/10.1088/0031-9155/53/23/001.

30. J. S. Bredfeldt, Y. M. Liu, C. A. Pehlke, et al., "Computational Segmentation of Collagen Fibers From Second-Harmonic Generation Images of Breast Cancer," *Journal of Biomedical Optics* 19, no. 1 (2014): 016007, https://doi.org/10.1117/1.jbo.19.1.016007.

31. A. Uchugonova, M. Zhao, M. Weinigel, et al., "Multiphoton Tomography Visualizes Collagen Fibers in the Tumor Microenvironment That Maintain Cancer-Cell Anchorage and Shape," *Journal of Cellular Biochemistry* 114, no. 1 (2013): 99–102, https://doi.org/10.1002/jcb.24305.

32. S. B. Ned Bowden, A. G. Evans, J. W. Hutchinson, and G. M. Whitesides, "Spontaneous Formation of Ordered Structures in Thin Films of Metals Supported on an Elastomeric Polymer," *Nature* 393, no. 6681 (1998): 6146–6149, https://doi.org/10.1038/30193.

33. J. M. Caves, V. A. Kumar, W. J. Xu, N. Naik, M. G. Allen, and E. L. Chaikof, "Microcrimped Collagen Fiber-Elastin Composites," *Advanced Materials* 22, no. 18 (2010): 2041–2044, https://doi.org/10.1002/adma.200903612.

34. J. Sapudom, S. Rubner, S. Martin, et al., "The Phenotype of Cancer Cell Invasion Controlled by Fibril Diameter and Pore Size of 3D Collagen Networks," *Biomaterials* 52 (2015): 367–375, https://doi.org/10.1016/j.biomaterials.2015.02.022.

35. C. J. Lowe, I. M. Reucroft, M. C. Grota, and D. I. Shreiber, "Production of Highly Aligned Collagen Scaffolds by Freeze-Drying of Self-Assembled, Fibrillar Collagen Gels," *ACS Biomaterials Science & Engineering* 2, no. 4 (2016): 643–651, https://doi.org/10.1021/acsbiomaterials.6b00036.

36. X. S. Luo, Z. Z. Guo, P. He, et al., "Study on Structure, Mechanical Property and Cell Cytocompatibility of Electrospun Collagen Nanofibers Crosslinked by Common Agents," *International Journal of Biological Macromolecules* 113 (2018): 476–486, https://doi.org/10.1016/j.ijbiomac.2018.01.179.

37. S. Moroi, T. Miura, T. Tamura, X. Zhang, K. Ura, and Y. Takagi, "Self-Assembled Collagen Fibrils From the Swim Bladder of Bester Sturgeon Enable Alignment of MC3T3-E1 Cells and Enhance Osteogenic Differentiation," *Materials Science & Engineering, C: Materials for Biological Applications* 104 (2019): 109925, https://doi.org/10.1016/j.msec.2019.109925.

38. M. Plodinec, M. Loparic, C. A. Monnier, et al., "The Nanomechanical Signature of Breast Cancer," *Nature Nanotechnology* 7, no. 11 (2012): 757–765, https://doi.org/10.1038/nnano.2012.167.

39. E. S. Lai, N. F. Huang, J. P. Cooke, and G. G. Fuller, "Aligned Nanofibrillar Collagen Regulates Endothelial Organization and Migration," *Regenerative Medicine* 7, no. 5 (2012): 649–661, https://doi.org/10.2217/rme.12.48.

40. J. a. M. Nuhn, A. M. Perez, and I. C. Schneider, "Contact Guidance Diversity in Rotationally Aligned Collagen Matrices," *Acta Biomaterialia* 66 (2018): 248–257, https://doi.org/10.1016/j.actbio.2017.11.039.

41. K. M. Riching, B. L. Cox, M. R. Salick, et al., "3D Collagen Alignment Limits Protrusions to Enhance Breast Cancer Cell Persistence," *Biophysical Journal* 107, no. 11 (2014): 2546–2558, https://doi.org/10.1016/j.bpj.2014.10.035.

42. M. W. Conklin, J. C. Eickhoff, K. M. Riching, et al., "Aligned Collagen is a Prognostic Signature for Survival in Human Breast Carcinoma," *American Journal of Pathology* 178, no. 3 (2011): 1221–1232, https://doi.org/10.1016/j.ajpath.2010.11.076.

43. A. Pathak and S. Kumar, "Independent Regulation of Tumor Cell Migration by Matrix Stiffness and Confinement," *Proceedings of the National Academy of Sciences of the United States of America* 109, no. 26 (2012): 10334–10339, https://doi.org/10.1073/pnas.1118073109.

44. L. Breideband, K. N. Wachtershauser, R. Sarkar, M. Puspathasan, E. H. K. Stelzer, and F. Pampaloni, "Gravitational Forces and Matrix Stiffness Modulate the Invasiveness of Breast Cancer Cells in Bioprinted Spheroids," *Materials Today Bio* 31 (2025): 101640, https://doi.org/10.1016/j.mtbio.2025.101640.

45. R. W. Tilghman, C. R. Cowan, J. D. Mih, et al., "Matrix Rigidity Regulates Cancer Cell Growth and Cellular Phenotype," *PLoS One* 5, no. 9 (2010): e12905, https://doi.org/10.1371/journal.pone.0012905.

46. B. A. Morris, B. Burkel, S. M. Ponik, et al., "Collagen Matrix Density Drives the Metabolic Shift in Breast Cancer Cells," *EBioMedicine* 13 (2016): 146–156, https://doi.org/10.1016/j.ebiom.2016.10.012.

47. F. Lin, H. H. Zhang, J. Y. Huang, and C. Y. Xiong, "Substrate Stiffness Coupling TGF-β1 Modulates Migration and Traction Force of MDA-MB-231 Human Breast Cancer Cells in Vitro," *ACS Biomaterials Science & Engineering* 4 (2018): 1337–1345, https://doi.org/10.1021/acsbiomaterials.7b00835.

48. M. J. Paszek, N. Zahir, K. R. Johnson, et al., "Tensional Homeostasis and the Malignant Phenotype," *Cancer Cell* 8, no. 3 (2005): 241–254, https://doi.org/10.1016/j.ccr.2005.08.010.

49. H. W. Lv, L. S. Li, M. Y. Sun, et al., "Mechanism of Regulation of Stem Cell Differentiation by Matrix Stiffness," *Stem Cell Research & Therapy* 6, no. 1 (2015): 103, https://doi.org/10.1186/s13287-015-0083-4.

50. K. Nagayama, K. Uchida, and A. Sato, "A Novel Micro-Grooved Collagen Substrate for Inducing Vascular Smooth Muscle Differentiation Through Cell Tissue Arrangement and Nucleus Remodeling," *Journal of the Mechanical Behavior of Biomedical Materials* 90 (2019): 295–305, https://doi.org/10.1016/j.jmbbm.2018.10.005.

51. J. N. Amens, G. Bahçecioglu, K. Dwyer, et al., "Maternal Obesity Driven Changes in Collagen Linearity of Breast Extracellular Matrix Induces Invasive Mammary Epithelial Cell Phenotype," *Biomaterials* 297 (2023): 122110, https://doi.org/10.1016/j.biomaterials.2023.122110.

52. A. Isomursu, K. Y. Park, J. Hou, et al., "Directed Cell Migration Towards Softer Environments," *Nature Materials* 21, no. 9 (2022): 1081–1090, https://doi.org/10.1038/s41563-022-01294-2.

53. Z. Z. Mai, Y. F. Lin, P. Lin, X. Y. Zhao, and L. Cui, "Modulating Extracellular Matrix Stiffness: A Strategic Approach to Boost Cancer Immunotherapy," *Cell Death & Disease* 15, no. 5 (2024): 307, https://doi.org/10.1038/s41419-024-06697-4.

54. E. Cambria, M. F. Coughlin, M. A. Floryan, G. S. Offeddu, S. E. Shelton, and R. D. Kamm, "Linking Cell Mechanical Memory and Cancer Metastasis," *Nature Reviews Cancer* 24, no. 3 (2024): 216–228, https://doi.org/10.1038/s41568-023-00656-5.

55. Y. D. Ning, M. Y. Zheng, Y. Zhang, Y. Q. Jiao, J. P. Wang, and S. W. Zhang, "RhoA-ROCK2 Signaling Possesses Complex Pathophysiological Functions in Cancer Progression and Shows Promising Therapeutic Potential," *Cancer Cell International* 24, no. 1 (2024): 339, https://doi.org/10.1186/s12935-024-03519-7.

56. C. M. Lo, H. B. Wang, M. Dembo, and Y. L. Wang, "Cell Movement is Guided by the Rigidity of the Substrate," *Biophysical Journal* 79, no. 1 (2000): 144–152, https://doi.org/10.1016/s0006-3495(00)76279-5.

57. D. E. Discher, P. Janmey, and Y. L. Wang, "Tissue Cells Feel and Respond to the Stiffness of Their Substrate," *Science* 310, no. 5751 (2005): 1139–1143, https://doi.org/10.1126/science.1116995.